HHS Public Access

Author manuscript

Cancer Res. Author manuscript; available in PMC 2020 March 15.

Published in final edited form as:

Cancer Res. 2019 September 15; 79(18): 4787–4797. doi:10.1158/0008-5472.CAN-19-0530.

A near-infrared phosphorescent nanoprobe enables quantitative, longitudinal imaging of tumor hypoxia dynamics during radiotherapy

Xianchuang Zheng[1], **Liyang Cui**[1], **Min Chen**[1], **Luis A. Soto**[2], **Edward E. Graves**[2], **Jianghong Rao**[1,*]

[1]Department of Radiology, Molecular Imaging Program at Stanford, School of Medicine, Stanford University, Stanford, CA 94305, USA.

[2]Department of Radiation Oncology, Molecular Imaging Program at Stanford, School of Medicine, Stanford University, Stanford, CA 94305, USA.

Abstract

Hypoxia plays a key role in tumor resistance to radiotherapy (RT). It is important to study hypoxia dynamics during RT to improve treatment planning and prognosis. Here, we describe a luminescent nanoprobe, composed of a fluorescent semiconducting polymer and palladium (Pd) complex, for quantitative longitudinal imaging of tumor hypoxia dynamics during RT. The nanoprobe was designed to provide high sensitivity and reversible response for the subtle change in hypoxia over a narrow range (0-30 mmHg O_2), which spans the oxygen range where tumors have limited radiosensitivity. Following intravenous administration, the nanoprobe efficiently accumulated in and distributed across the tumor, including the hypoxic region. The ratio between emissions at 700 and 800 nm provided quantitative mapping of hypoxia across the entire tumor. The nanoprobe was used to image tumor hypoxia dynamics over 7 days during fractionated RT, and revealed that high fractional dose (10 Gy) was more effective in improving tumor reoxygenation than low dose (2 Gy) and the effect tended to persist longer in smaller or more radiosensitive tumors. Our results also indicated the importance of the reoxygenation efficiency of the first fraction in the prediction of the radiation treatment outcome. In summary, this work has established a new nanoprobe for highly sensitive, quantitative and longitudinal imaging of tumor hypoxia dynamics following RT, and demonstrated its value for assessing the efficacy of RT and radiation treatment planning.

Keywords

Hypoxia; radiotherapy; oxygen sensing; nanoprobe; ratiometric imaging

*Corresponding Author. jrao@stanford.edu; 1201 Welch Road, Lucas Center P093, Stanford, CA 94305-5484; Tel: 1-650-736-8563.

Disclosure of Potential Conflicts of Interest

No potential conflicts of interest were disclosed.

Introduction

Hypoxia is a characteristic feature of most solid tumors and plays a crucial role in their resistance to cancer treatment, especially radiotherapy (RT) (1,2). Tumor hypoxia can reduce DNA damage caused by radiation and promote tumor cell survival via hypoxia-inducible factor regulated pathways (3,4), but can also compromise the repair of DNA damage (5,6). Hypoxia has become a major focus of efforts to improve the prognosis and treatment planning of RT (7), and multiple strategies have been developed to improve the RT efficacy by targeting hypoxia (8,9). On the other hand, RT itself can also induce changes in tumor oxygenation and the spatiotemporal complexity of this process remains poorly understood (10,11). Understanding the dynamic change of tumor hypoxia during RT requires noninvasive, real-time imaging of hypoxia over a long period of time as opposed to the single timepoint measurements. This is especially important for fractionated RT as the change of hypoxia induced by prior fractions will impact the effectiveness of the following fractions.

The oxygen electrode has been the ‘gold standard’ to measure tumor hypoxia but is invasive and limited to easily accessible tumors (12). Because of tumor heterogeneity, multiple locations may have to be sampled in order to precisely map hypoxia across an entire tumor. Molecular imaging methods can provide noninvasive measurement of tumor hypoxia through the use of hypoxia-responsive imaging probes. For example, positron emission tomography (PET), functional magnetic resonance imaging (fMRI), and photoacoustic (PA) imaging (13-16) have been applied to image hypoxia during RT. Optical imaging of hypoxia is attractive due to its high sensitivity and ease of use. Optical spectroscopy such as the diffuse reflection spectroscopy (DRS) has been successfully employed for imaging tumor hypoxia by measuring the saturation of endogenous hemoglobin (17), which mainly reports the oxygenation level in the blood vessels. Exogenous optical imaging probes have been developed to measure hypoxia beyond the blood vessels. Among hypoxia-responsive optical imaging probes, phosphorescent transition metal complexes have drawn great attention for their reversible and sensitive response to the change of hypoxia (18,19). Phosphorescence lifetime imaging can directly quantify the hypoxia level using the time-resolving camera (20-23). Alternatively, ratiometric imaging probes are reported by integrating the phosphor with an internal reference for ratiometric imaging of hypoxia. Semiconducting polymers (SP) can be an excellent candidate for the internal reference due to its better photostability than small molecule dyes (24,25) and lower *in vivo* toxicity than inorganic quantum dots (26). However, currently reported ratiometric imaging probes based on SP and phosphor need UV light excitation and emit in the visible range, thus are not suitable for *in vivo* study of tumor hypoxia (27,28). Here, we report a new ratiometric hypoxia luminescent imaging (RHyLI) nanoprobe based on SP and phosphor that can be excited with red light and exhibit dual near-infrared (NIR) emissions. We show that the RHyLI nanoprobe can efficiently penetrate into the hypoxic regions of the tumor tissues after systemic administration and allow for quantitative imaging of tumor hypoxia dynamics during RT over a period of one week. We demonstrate the effects of multiple factors on evolution pattern of tumor hypoxia during fractionated RT. Interestingly, our results have revealed the importance of the first

fraction in controlling the reoxygenation efficiency of tumor and tumor hypoxia level and thus tumor growth.

Materials and Methods

Synthesis of the RHyLI nanoprobe

Semiconducting polymer PFO-DBT (0.25 mg), Pd complex (Pd-TPTBP) (25 μg), and poly(styrene-b-ethylene oxide) (0.5 mg) were dissolved in THF (2 mL), and then rapidly injected to distilled water (10 mL) under sonication in a Branson 1800 ultrasonic cleaner. After further sonicated for 2 min, THF was removed and the aqueous suspension was washed three times with distilled water by ultra-centrifugation. The final concentration of PFO-DBT and Pd complex in the obtained nanoprobe aqueous suspension was determined by the absorption and ICP-MS measurements, respectively. The concentration of the nanoprobe was described by the total mass concentration of the PFO-DBT and the Pd complex. The probe response to oxygen (0, 2.1, 4.2, 6.3, 8.4, 10.5, 14.7, and 21%) was measured by collecting the emission spectra (650–850 nm) on a Horiba Jobin Yvon FluoroMax-3 spectrofluorometer at 630 nm excitation.

Cell culture

HeLa, H460, H1299, A549 and RWPE-1 cells (all were obtained from ATCC between 2013 and 2018 without further authentication) were cultured under 5% CO_2 and 95% humidified air at 37 °C. The complete growth media were RPMI medium 1640 (GIBCO) containing L-Glutamine, 25 nM HEPES and 10% fetal bovine serum (FBS, GIBCO) for HeLa, H460 and H1299 cells, DMEM (Corning) supplemented with 10% FBS and 1% Pen/Strep (Fisher Bioreagents) for A549 cells, and Keratinocyte Serum Free Medium (K-SFM) supplied with bovine pituitary extract (BPE, 0.05 mg/mL) and human recombinant epidermal growth factor (EGF, 5 ng/mL) for RWPE-1 cells. Mycoplasma was monthly evaluated by using PCR Mycoplasma Detection Kit (Alfa Aesar).

Animal experiments

All animal experiments were performed in compliance with the Guidelines for the Care and Use of Research Animals established by the Stanford University Institutional Animal Care and Use Committee with NU/NU nude mice (5–6 weeks, Charles River Laboratories International, Inc.). Mice were randomly assigned to treatment groups. The investigators were not blind to the groups during data acquisition and analysis due to limited available personnel during animal experiments.

Tumor models

For tumor implantation, each NU/NU nude mouse was subcutaneously injected with 100 μL of cell suspension in PBS (containing 50% Corning Matrigel): 10^6 for HeLa and H460 cells, 2×10^6 for H1299 cells, and 5×10^6 cells for A549 cells. The implantation was either on the right rear thigh of the mice (HeLa, H460, and H1299) or on the middle right side of the back (A549). The tumor growth was monitored every other day or daily by measuring the tumor size with a digital caliper.

Measuring oxygen partial pressure (PO_2) with oxygen microelectrode

A needle-type oxygen microelectrode (Unisense, OX-100) with a tip size of 100 μm was held on a Stoelting Just for Mouse™ Stereotaxic Instrument. The oxygen microelectrode was connected to an amplifier (OXY-Meter, Unisense) and then to a computer for recording. Pre-polarization of the microelectrode was performed according to the manufacturer instruction for 4 hours. The microelectrode calibration was done with the distilled water bubbled with air or argon for 5 min in a calibration chamber. To measure the PO_2 in tumor tissues, tumor-bearing mice were anaesthetized with isoflurane (1.5%) and fixed on the plate of the stereotaxic instrument. The microelectrode was inserted into the tumor tissues and moved stepwise (0.5 mm per step) by using the micro-manipulator of the stereotaxic instrument to measure the PO_2 from the surface to the core at each spot. PO_2 was recorded after waiting for 10 s for stable readouts at each step and reported as an average of five separate spots. Since the microelectrode may perturb local O_2 field by consuming O_2, in this study, the microelectrode was used to measure PO_2 in tumors at a single time point instead of tracking PO_2 of the same tumor over time.

Ratiometric imaging of tumor hypoxia

Tumor-bearing mice were imaged in an IVIS spectrum *in vivo* imaging system after administration of the RHyLI nanoprobe (100 μL PBS, 2 mg/kg). The photoluminescence signals were collected at 700 nm (690–710 nm filter) and 800 nm (790–810 nm filter) with the excitation 620–660 nm filter. The gray images were imported into Matlab (v9.0.0, MathWorks) to generate ratiometric images by dividing the intensity at the 800 nm by the intensity at the 700 nm pixel-to-pixel (I_{800}/I_{700}–1). In each ratiometric image, the tumor region was selected according to the corresponding brightfield image and the mean intensity of all the pixels in the tumor region was calculated (pixel size 0.196×0.196 mm, 1,306 pixels for a typical 8 mm tumor) and termed as ‘mean ratio’ to represent the average hypoxia level of the tumor. No extra correction was performed for partial volume effect.

Radiation treatment

Radiation therapy was performed on a Kimtron Polaris MC-500 X-ray irradiator at 225 kV and 13.3 mA with the dose rate of 0.01 Gy/s. Mice were anesthetized by intraperitoneal injection of 100 μL of ketamine hydrochloride (8 mg/mL) and xylazine (1.3 mg/mL) and placed on the work surface at 60 cm below the red dot on side of the cylinder head. Only the tumor tissues were irradiated by using a lead shield for blocking, and no more than 5 mice were irradiated together at each time point.

Imaging the tumor hypoxia dynamics in RT

Tumor-bearing mice were i.v. injected with the RHyLI nanoprobe in 100 μL PBS (2 mg/kg) and imaged at 24 h p.i. Then the mice were treated with the first RT fraction on a Kimtron Polaris MC-500 X-ray irradiator, and imaged at 0.5, 2, 4, 6, 8, 24, and 48 h after RT before next treatment and imaging cycle. Typically, there were three cycles of pre-RT imaging, RT, and post-RT imaging over time (0.5–48 h).

To explore the correlation between tumor hypoxia and tumor growth, NU/NU nude mice bearing H460 tumors on the right rear thigh (size 2-4 mm, n = 20) were randomly assigned

to two groups (n = 10 per group) and received two RT fractions at day 0 and day 2 (Group 1: 2 Gy + 10 Gy; Group 2: 10 + 2 Gy). The nanoprobe was i.v. injected at 24 h before the 1st RT fraction (2 mg/kg) for NIR ratiometric imaging of tumor hypoxia from day 0 to day 3, and the tumor size was recorded daily for 15 days.

Statistical analysis

Statistical analysis was performed using GraphPad Prism (v7.0, GraphPad Software, Inc.). Comparison between two groups was performed by two-tailed t-test with Welch's correction, assuming Gaussian distribution. Comparisons among three groups were performed by one-way ANOVA with Geisser-Greenhouse correction. * $p < 0.05$, ** $p < 0.01$. A p value < 0.05 was considered to be statistically significant. The results are presented as Mean ± SD.

Results

Synthesis and photophysical properties of the nanoprobe

The RHyLI nanoprobe was prepared based on a palladium (Pd) complex and a fluorescent SP (PFO-DBT) using the nanoprecipitation method (29) (Fig. 1A). The phosphorescence of the Pd complex is extremely sensitive to oxygen (30), making it highly valuable for sensing subtle changes of hypoxia at low oxygen levels. The SP serves as the internal reference for ratiometric imaging due to its stable and oxygen-insensitive fluorescence property (31) as well as the matrix for encapsulating the Pd complex. The synthesized nanoprobe showed a diameter of 17±4 nm by TEM (Fig. 1B, C), and a hydrodynamic diameter of 28±7 nm in aqueous solution by DLS (Fig. 1D). The mean zeta-potential of the nanoprobe in PBS (1×, pH 7.4) was determined to be −7 mV (Supplementary Fig. S1). The stability of the nanoprobe was followed for 30 days in PBS (1×, pH 7.4) at 4 ºC by DLS, and little change in the hydrodynamic diameter of the particles was observed (Fig. 1E).

The nanoprobe exhibited a broad absorption in the visible range up to 650 nm (Supplementary Fig. S2). When excited at 630 nm, the nanoprobe emitted maximally at 685 and 795 nm from the SP and Pd complex, respectively (Fig. 1F). The red excitation and near-infrared (NIR) emissions make it suitable for *in vivo* imaging. The phosphorescence emission at 795 nm increased when the oxygen level decreased—as high as 13.5-fold when the oxygen level dropped to 0 from 21%, while the emission at 685 nm remained nearly unchanged. The ratio of the emission intensity between 795 and 685 nm ($R_{795/685}$) increased nonlinearly as the oxygen level decreased, with the sharpest response in the low oxygen range (e.g. 0–4% O_2) (Fig. 1G). As the oxygen levels of hypoxic tumors have been reported to vary between 0–3% in both clinical and preclinical studies, and the sensitivity of tumors to RT begins to decrease with decreasing oxygen at a threshold of 3.3–3.9% O_2 (1), the large response range of the probe over a narrow oxygen range (0–4%) is well-suited to detect hypoxia-mediated changes in radiosensitivity (< 3.9% O_2). Importantly, this ratiometric approach cancelled out variations in probe concentration in different tumors and different regions of tumors in quantifying hypoxia.

The response of the phosphorescence emission of the Pd complex to oxygen is based on energy transfer from the triplet excited state of the Pd complex to the triplet ground state of molecule oxygen (32), therefore, the response of the nanoprobe to the oxygen level was fully reversible (Fig. 1H), unlike 2-nitroimidazole based PET and immunohistochemistry probes that irreversibly form adducts with biomolecules after reduction (33,34). The RHyLI nanoprobe exhibited nearly no response to other stimuli, including pH (3-9), hydrogen peroxide (up to 32 μM), and hydroxyl radical (up to 8 μM) (Supplementary Fig. S3A, B, C). The uptake of the RHyLI nanoprobe (5 μg/mL) in HeLa cells indicated strong red fluorescence signal in confocal imaging (Supplementary Fig. S4A).

The response of the RHyLI nanoprobe to tumor hypoxia

After testing the cytotoxicity of the RHyLI nanoprobe in HeLa (Supplementary Fig. S4B) and RWPE-1 cells (Supplementary Fig. 5A, B, C), we evaluated its response to the hypoxic conditions of solid tumors. As shown in Supplementary Fig. S6A, same amount of the nanoprobe (0.1 mg/mL in 40 μL PBS) was injected into the HeLa tumor xenograft on the right rear thigh and normal tissue on the contralateral thigh of a nude mouse for NIR ratiometric imaging. To corroborate the hypoxia measurement from the ratiometric image, oxygen partial pressures (PO_2) in tumor and normal tissues were directly measured using a needle-type oxygen microelectrode, showing an excellent correlation with RHyLI (Supplementary Fig. S6B). The emission spectra of the signals from tumor and normal tissues indicated that the 800 nm signal was selectively enhanced in the hypoxic tumor tissue (Supplementary Fig. S6C), which agrees with the *in vitro* hypoxia response of the nanoprobe (Fig. 1F).

Intravenous (i.v.) administration of the probe is generally preferred to intratumoral delivery for *in vivo* imaging. We first validated that intravenously injected nanoprobe was able to sufficiently accumulate in and efficiently distribute across tumors, including both perfused and hypoxic regions. Nude mice bearing HeLa tumors (N = 3) were i.v. injected with the nanoprobe (2 mg/kg) and sacrificed 24 h later to quantify the biodistribution of the nanoprobe by *ex vivo* imaging in the 700 nm channel (Supplementary Fig. S7A) as well as ICP-MS analysis of Pd (Supplementary Fig. S7B). ICP-MS showed the probe accumulation in tumor tissues of 7.4±1.6% ID/g tissue, which is higher than the average level reported for nanomedicines (35).

To characterize the delivery of the nanoprobe across the tumor, the excised HeLa tumors were processed for immunofluorescence staining. The frozen sections of the tumor tissues were stained with CD31 and pimonidazole (PIMO) antibody (green) to reveal the tumor blood vessels and hypoxic regions of the tumors, respectively (Fig. 2A, B). The distribution of the nanoprobe within the tumor tissues was followed by its fluorescence signal at the 700 nm channel (red). Three different regions of the tumor including periphery (exhibiting the most abundant blood vessels and lowest hypoxia staining), semi-periphery (0–400 μm away from the periphery), and center were analyzed in the selected regions of interest (ROI 1&2 in Fig. 2A, B). From the periphery to the semi-periphery to the center, the tumor vasculature density (CD31 staining per area) decreased by 83% and 72%, and the hypoxia level (PIMO staining per area) increased by 4.5- and 7.1-fold, while the nanoprobe concentration

decreased to 41–45% and 54–61% of that in the periphery, respectively (Fig. 2C, D). The ratio of the probe concentration to the vascular density in the semi-periphery and the center was found to be 2.4- and 1.9-fold higher than that in the periphery ($p<0.01$), respectively (Fig. 2E), indicating that although the semi-periphery and the center of the tumor tissue have relatively low vascular density, the blood vessels in these regions tend to be more efficient in the delivery of nanoprobes, likely due to their defective structure in the hypoxic regions of the tumors (36,37). As shown in Fig. 2F, G, the nanoprobe could extravasate from the blood vessels and penetrate into the hypoxic regions. Similar results were also observed when the nanoprobe was tested in H460 tumors (Supplementary Fig. S8A, B). As hypoxia in solid tumors is known highly heterogenous, the effective distribution of the RHyLI nanoprobe across the tumor including non-hypoxic and various hypoxic conditions (moderate to severe) renders it suitable for *in vivo* hypoxia measurement.

Longitudinal, reversible imaging of tumor hypoxia by RHyLI

Next, the nanoprobe (2 mg/kg) was injected intravenously into nude mice bearing HeLa tumor (6 mm) for hypoxia imaging. NIR ratiometric imaging was performed at various time points (1, 4, 8, 24, 48 h, and 7 days p.i.) (Fig. 3A). The tumor signals in the 700 nm channel showed prolonged retention of the nanoprobe in the tumor for 7 days after a single i.v. injection (Fig. 3B), indicating its ability to longitudinally image tumor hypoxia. The ratiometric images reported the level of tumor hypoxia (Fig. 3C). The “mean ratio” (the mean intensity of all the pixels in the tumor in the ratiometric image) was calculated to represent the mean hypoxia conditions of the tumor, which should be contributed by both intracellular and extracellular oxygen considering the cell uptake of the nanoprobes (Supplementary Fig. S4).

Using the RHyLI nanoprobe, we compared the hypoxia levels in different tumor sizes and types. The nanoprobe was i.v. injected to nude mice bearing HeLa tumors at different sizes (2, 6, 10, or 16 mm, Fig. 3D, Supplementary Fig. S9) or different types of tumor (HeLa, H460, and H1299) at the same size (8 mm) (Fig. 3E, Supplementary Fig. S10), followed by tumor hypoxia imaging at 24 h p.i. The size-dependent hypoxic conditions were observed in the HeLa tumors (Fig. 3F), and the H1299 tumors showed relatively moderate hypoxic conditions as compared to HeLa and H460 tumors (Fig. 3G). All these measurements with RHyLI were confirmed by oxygen microelectrode (Fig. 3H, I). These results show that RHyLI can effectively image oxygen levels in the range of 1–27 mmHg (Fig. 3H, I).

To test the reversibility of the RHyLI nanoprobe to hypoxia *in vivo*, the HeLa tumor and normal tissues were tied with a string to restrict blood flow and induce severe hypoxia, followed by removal of the string to allow recovery of blood circulation and oxygenation (Fig. 3J, Supplementary Fig. S11). The mean ratio reported by ratiometric imaging showed an increase and then decrease over the course of this procedure (Fig. 3K), confirming the reversibility of the nanoprobe response to changes in hypoxia *in vivo*. The reciprocal of mean ratio showed a linear correlation with the oxygen partial pressure (PO_2 in mmHg) measured with the oxygen microelectrode (Fig. 3L), allowing quantification of hypoxia within a tumor by ratiometric imaging with the RHyLI.

Imaging tumor hypoxia dynamics during radiotherapy (RT)

After validating the stability of the nanoprobe upon radiation (Supplementary Fig. S12A, B), we then imaged the tumor hypoxia dynamics over the course of fractionated RT. Typically, tumor-bearing nude mice were treated with three RT fractions (2 or 10 Gy per fraction) with an interval of 48 h and tumor hypoxia was noninvasively imaged throughout the RT treatment period for 144 h (Fig. 4A). The nanoprobe was i.v. injected to mice (2 mg/kg) at 24 h before the first RT fraction. When HeLa tumors (8 mm) were treated with the first RT fraction at a high dose (10 Gy), the mean ratio increased from 0.280±0.041 pre-RT to 0.442±0.078 at 0.5 h after RT and then gradually decreased to 0.147±0.042 at 24 h after RT (Fig. 4B, C). These mean ratios corresponded to the mean PO_2 of 3.02±0.43 mmHg pre-RT, 1.99±0.32 mmHg at 0.5 h and 5.44±1.16 mmHg at 24 h after RT. This result confirms that the RHyLI nanoprobe can report the subtle dynamic change of tumor hypoxia induced by RT.

The measured oxygen levels for HeLa tumors treated with three RT fractions at different doses (10 or 2 Gy per fraction) reveal that RT first induced a transient increase in tumor hypoxia, followed by a progressive reoxygenation (Fig. 4C, D, Supplementary Fig. S13). The observed reoxygenation in tumors induced by RT agrees with previous studies with the oxygen electrode measurement (3,38). However, although reoxygenation is often the dominating trend in the initial period after RT (e.g. 0.5–24 h), the long-term evolution of tumor hypoxia with an interval of 24 h is not always declining and may vary depending on the RT dose (Fig. 4E). For instance, a high RT dose (10 Gy) decreased the mean ratio from 0.280±0.041 pre-RT to 0.147±0.042 at 24 h after the first RT fraction ($p<0.01$) but increased to 0.307±0.031 after the third RT fraction (at 144 h). However, a small fractional RT dose (2 Gy) increased the mean ratio from 0.293±0.032 pre-RT to 0.446±0.035 at 48 h after the first RT fraction ($p<0.01$).

The long-term evolution of tumor hypoxia obtained by ratiometric imaging can provide valuable predictive information for the treatment effect of RT, since the change of tumor hypoxia induced by the prior RT fraction will directly impact the effectiveness of subsequent fractions. Tumor response as measured by change in tumor volume demonstrated that the high RT dose but not the low RT dose resulted in tumor control (Fig. 4F). On the other hand, the short-term dramatic change of tumor hypoxia in the first 24 h after each fraction monitored by ratiometric imaging can reflect the combined effects of multiple factors on oxygenation such as radiation-induced direct and indirect cell death, changes in blood perfusion, acute and chronic vascular damage, change of interstitial fluid pressure (IFP), and tumor stromal fibrosis (3,39) (Fig. 4C, D). These factors may modulate oxygenation in contradictory ways. To quantify the combined contributions of these factors, we proposed the use of a term--reoxygenation efficiency, defined by the ratio of the decrease in hypoxia during the reoxygenation-dominated period (0.5–24 h) (difference between the mean ratio at 0.5 h and at 24 h) to the increase in hypoxia immediately after RT (0–0.5 h) (difference between the mean ratio at 0.5 h after RT and pre-RT). Fig. 4G shows that high RT doses (10 Gy) produced better reoxygenation efficiency than low doses (2 Gy) in the first fraction (1.82±0.34 for high dose versus 0.56±0.12 for low dose), but the difference in subsequent fractions was small between high and low doses. This result suggests the importance of the

first fraction and its dose in controlling the reoxygenation efficiency and thus tumor hypoxia level.

To investigate the effect of tumor growth stage on the hypoxia dynamics during RT, HeLa tumors of a small size (5 mm) were treated with three high dose RT fractions (10 Gy per fraction) and imaged with the RHyLI nanoprobe. The evolution of tumor hypoxia over time (Fig. 5A, Supplementary Fig. S14) was compared to that of a larger tumor (8 mm) with the same treatment (Fig. 4C), showing a significant difference in the periods of the second and third RT fractions (Fig. 5B). For the large tumors, the two subsequent RT fractions induced an increase of the mean ratio from 0.175±0.038 before the second RT fraction (at 48 h) to 0.307±0.031 at 144 h ($p<0.01$). For the smaller tumors, however, the mean ratio showed no significant change from 0.192±0.030 at 48 h to 0.172±0.021 at 144 h ($p>0.05$). This result indicates that while the first fraction of large dose radiation improved tumor reoxygenation, the improvement tended to persist longer in small tumors than large tumors during the course of RT.

The dynamics of tumor hypoxia during RT were also studied in different tumor types. H460 tumors (8 mm) were treated with three high dose RT fractions (10 Gy per fraction). The evolution of tumor hypoxia was monitored over one week (Fig. 5C, Supplementary Fig. S15) and compared with the result of HeLa tumors with the same tumor size and RT dose (Fig. 4C). While H460 tumor cells are known to being radiosensitive and HeLa radioresistant (40,41), they showed similar hypoxia levels before the first RT fraction (mean ratio 0.280±0.041 for HeLa versus 0.301±0.070 for H460; Fig. 5D) and their long-term evolution trend was similar in the first fraction period (0–48 h). However, in the two subsequent RT fractions (48–144 h), tumor hypoxia started to increase in HeLa tumors but not in H460 tumors. H460 tumors exhibited higher reoxygenation efficiency than HeLa tumors in the second and third RT fractions (Fig. 5E). This result implies that intrinsic characteristics of tumor cells may play a key role in defining the evolution of hypoxia in response to fractionated RT. While the first fraction of large dose radiation improved tumor reoxygenation in both radiosensitive and radioresistant tumors, subsequent fractions produced more efficient reoxygenation in radiosensitive tumors than in radioresistant tumors.

The effects of the first RT fraction on tumor hypoxia dynamics and treatment outcome were tested on H460 tumor xenografts. Nude mice bearing H460 tumors (2-4 mm) were i.v. injected with the RHyLI nanoprobe (2 mg/kg) before treated with two RT fractions (group 1: 2 Gy + 10 Gy; group 2: 10 Gy + 2 Gy; n = 10 mice per group, Fig. 5F). The tumor hypoxia was monitored for the first 3 days and the tumor growth was measured over 15 days. Group 1 and 2 had similar tumor hypoxia levels before RT (mean ratio 0.176±0.045 vs 0.171±0.058, Fig. 5G). But the mean ratio increased to 0.472±0.104 (group 1) vs 0.231±0.067 (group 2) at 24 h after the first RT fraction and 0.482±0.089 (group 1) vs 0.211±0.046 (group 2) at 24 h after the second RT fraction. Therefore, even with the same total radiation dose, a higher dose in the first fraction (group 2) led to a lower tumor hypoxia level (smaller ratio) and slower tumor growth (Fig. 5H).

To further explore the correlation between tumor hypoxia and tumor growth of fractionated RT, the increase of tumor volume from day 0 to 15 was correlated with the hypoxia levels at various time points or the reoxygenation efficiency during the two RT fractions for each mouse in the two groups (n = 20, Supplementary Fig. S16A-E) (17). The tumor volume increase showed better correlation with the reoxygenation efficiency in the first fraction (P=0.0190) than that of the second fraction (P=0.4805). Besides, better correlation was observed for the hypoxia levels after RT (P=0.0706 after 1st fraction and 0.0472 after 2nd fraction) than that before RT (P=0.1883). These results suggest that the information of tumor hypoxia during fractionated RT, especially the reoxygenation efficiency after the first fraction, may be valuable for predicting treatment outcome.

Both HeLa and H460 tumors are very hypoxic, exhibiting a mean PO_2 of 3 mmHg at a tumor diameter of 8 mm (Fig. 3I). The mean ratio measured in these two tumors during RT ranged from 0.124 to 0.588, corresponding to PO_2s of 1.56 to 6.42 mmHg, representing severe hypoxia. To evaluate the RHyLI nanoprobe in tumors with moderate hypoxia, which have been frequently reported in clinical studies (1), H1299 tumors (8 mm, mean PO_2 26.4 mmHg) were treated with three RT fractions (10 Gy per fraction) and imaged with RHyLI (Supplementary Fig. S17&18). The mean ratio was found to vary in the range of 0.036–0.230 during RT, corresponding to a PO_2 range of 3.57–26.4 mmHg. Therefore, the RHyLI nanoprobe is able to image tumor hypoxia over an oxygen range of 1.56–26.4 mmHg *in vivo*.

To improve the effectiveness of RT, a variety of adjuvants are being developed to alleviate or compensate for tumor hypoxia. These can also be evaluated using the RHyLI nanoprobe. Nude mice bearing A549 tumors were treated with papaverine hydrochloride (PPV, 2 mg/kg) by i.v. injection, a drug that has been shown to inhibit mitochondrial complex 1 and correspondingly oxygen consumption in tumors to reduce tumor hypoxia (42). A gradual decrease in tumor hypoxia was observed by ratiometric imaging after drug administration (Supplementary Fig. S19A,B). The mean ratio decreased from 0.160 to 0.096, corresponding to an increase of PO_2 from 5.01 to 8.19 mmHg. This result agrees with the recent findings reported in the literature (42).

Discussion

In this work we have designed a new hypoxia imaging nanoprobe (RHyLI) that can quantitatively measure and monitor tumor hypoxia in real time over the course of RT. In comparison to existing hypoxia imaging probes, RHyLI offers several advantages: 1) RHyLI quantitatively measures oxygen levels by ratiometric imaging, in contrast to qualitative measurement of PET probes; 2) RHyLI provides direct and reversible measurement of hypoxia, in contrast to irreversible and nitroreductase-dependent response of 2-nitroimidazole based PET probes (33); 3) RHyLI uses NIR imaging that is nonradiative and low-cost; 4) RHyLI can report on the oxygen level beyond blood vessels, unlike fMRI and PA methods that measure hemoglobin oxygen saturation within vessels only (43,44); 5) RHyLI can facilitate long-term measurement of tumor hypoxia over one week; and 6) RHyLI is sensitive to oxygen levels between 1.56–26.4 mmHg and is particularly suited to imaging tumor hypoxia dynamics during RT. This hypoxia range (0–30 mmHg O_2) has been

reported to associate with positive or negative responses to RT. For example, patients with median tumor oxygen tensions of >10 mmHg exhibited post-RT disease-free survival rates of 78% v.s. <10 mmHg with 22% (45).

This novel approach towards imaging hypoxia *in vivo* has several limitations. Firstly, NIR imaging has a limited tissue penetration depth of a few centimeters, a major disadvantage in comparison to PET that limits it in the clinical setting to superficial targets, those accessible with an endoscope or intraoperative imaging. In the current study, the imaging of tumor hypoxia dynamics during RT was performed on the subcutaneous tumors with the diameter of 2 to 8 mm, which was within the penetration depth of NIR light. Furthermore, while the difference in wavelength between the constitutive and oxygen-sensitive channels allows their independent detection and quantitation, it also presents the possibility that the wavelength-dependent differences in tissue absorption and scattering may interfere with the quantification in ratiometric imaging. However, the quantification of tumor oxygenation in this work was calibrated with oxygen electrode measurement performed in animal (Fig. 3L), which should minimize the impact of wavelength-dependent tissue absorption and scattering. Finally, the nanoprobe needs to penetrate into the hypoxic regions of tumor tissues to measure the local hypoxia, which may be inefficient in some tumor types considering the multiple barriers for the penetration of nanoparticles (46). However, the nanoprobe can still report the hypoxia in or near the blood vessels, similar to the hypoxia imaging methods that measure hemoglobin oxygen saturation.

Longitudinal measurement of tumor hypoxia during RT with the RHyLI nanoprobe revealed a similar short-term evolution pattern in each RT fraction period regardless of tumor size, type, and RT dose, which was comprised of a transient increase in hypoxia followed by reoxygenation. Several factors may contribute to this pattern in combination, for example, acute damage to endothelial cells that are rapidly proliferating and inherently sensitive to radiation (47), the increased blood perfusion, reduced oxygen metabolism of tumor cells, decreased IFP, and HIF-1α-regulated angiogenesis (10,39,48). The long-term evolution of tumor hypoxia in fractionated RT was found to vary with RT dose, tumor size, and type. Higher fractional doses improved tumor reoxygenation efficiency, which persisted longer for smaller and more radiosensitive tumors. Our observations also indicate the importance of the first fraction in dictating the results of a fractionated course of RT. High reoxygenation efficiency in the first fraction can contribute to a relatively lower hypoxia level in all the follow-up fractions and has been found to be correlated with a better treatment outcome. In addition, the ability of the RHyLI nanoprobe to quantify small changes in tumor hypoxia in real time may also make it valuable for mechanistic studies of the effect of RT on tumor hypoxia as well as in the development of hypoxia-modulating drugs.

In summary, a new NIR ratiometric imaging nanoprobe (RHyLI) has been developed for quantitative and reversible measurement of hypoxia in the range of 0–30 mmHg. The nanoprobe was applied for imaging tumor hypoxia dynamics during fractionated RT at different radiation dose, tumor size and type. The first radiation fraction was found to be crucial for controlling the tumor hypoxia levels during fractionated RT and the reoxygenation efficiency in the first fraction might be key information for predicting radiation treatment outcome.

Supplementary Material

Refer to Web version on PubMed Central for supplementary material.

Acknowledgements

This work was supported by the NIH grant R01GM128089 and NCI CCNE-TD grant U54CA199075. The irradiator in Research Animal Facility (RAF) at Stanford was supported by NIH grant 1S10OD018208. TEM in Cell Sciences Imaging Facility (CSIF) at Stanford was supported by NIH grant 1S10RR02678001. We thank John Perrino for assisting with TEM imaging, Kitty Lee for assisting with confocal microscopy imaging, and Sunni R. Farley for the help in histology.

References

1. Hockel M, Vaupel P. Tumor hypoxia: definitions and current clinical, biologic, and molecular aspects. J Natl Cancer Inst 2001;93:266–76. [PubMed: 11181773]
2. Rankin EB, Giaccia AJ. Hypoxic control of metastasis. Science 2016;352:175–80. [PubMed: 27124451]
3. Barker HE, Paget JTE, Khan AA, Harrington KJ. The tumour microenvironment after radiotherapy: mechanisms of resistance and recurrence. Nat Rev Cancer 2015;15:409–25. [PubMed: 26105538]
4. Lomax ME, Folkes LK, O'Neill P. Biological consequences of radiation-induced DNA damage: relevance to radiotherapy. Clin Oncol 2013;25:578–85.
5. Bristow RG, Hill RP. Hypoxia, DNA repair and genetic instability. Nat Rev Cancer 2008;8:180–92. [PubMed: 18273037]
6. Kumareswaran R, Ludkovski O, Meng A, Sykes J, Pintilie M, Bristow RG. Chronic hypoxia compromises repair of DNA double-strand breaks to drive genetic instability. J Cell Sci 2012;125:189–99. [PubMed: 22266907]
7. Nordsmark M, Bentzen SM, Rudat V, Brizel D, Lartigau E, Stadler P, et al. Prognostic value of tumor oxygenation in 397 head and neck tumors after primary radiation therapy. An international multi-center study. Radiother Oncol 2005;77:18–24. [PubMed: 16098619]
8. Brown JM, Wilson WR. Exploiting tumour hypoxia in cancer treatment. Nat Rev Cancer 2004;4:437–47. [PubMed: 15170446]
9. Wilson WR, Hay MP. Targeting hypoxia in cancer therapy. Nat Rev Cancer 2011;11:393–410. [PubMed: 21606941]
10. Znati CA, Rosenstein M, Boucher Y, Epperly MW, Bloomer WD, Jain RK. Effect of radiation on interstitial fluid pressure and oxygenation in a human tumor xenograft. Cancer Res 1996;56:964–8. [PubMed: 8640786]
11. Kallman RF, Dorie MJ. Tumor oxygenation and reoxygenation during radiation theraphy: Their importance in predicting tumor response. Int J Radiat Oncol 1986;12:681–5.
12. Walsh JC, Lebedev A, Aten E, Madsen K, Marciano L, Kolb HC. The clinical importance of assessing tumor hypoxia: relationship of tumor hypoxia to prognosis and therapeutic opportunities. Antioxid Redox Signal 2014;21:1516–54. [PubMed: 24512032]
13. Metcalfe P, Liney GP, Holloway L, Walker A, Barton M, Delaney GP, et al. The potential for an enhanced role for mri in radiation-therapy treatment planning. Technol Cancer Res Treat 2013;12:429–46. [PubMed: 23617289]
14. Rich LJ, Seshadri M. Photoacoustic monitoring of tumor and normal tissue response to radiation. Sci Rep 2016;6:21237. [PubMed: 26883660]
15. Arabi M, Piert M. Hypoxia PET/CT imaging: implications for radiation oncology. Q J Nucl Med Mol Imaging 2010;54:500–9. [PubMed: 20927017]
16. Geets X, Grégoire V, Lee JA. Implementation of hypoxia PET imaging in radiation therapy planning. Q J Nucl Med Mol Imaging 2013;57:271–82. [PubMed: 24045623]
17. Hu F, Vishwanath K, Salama JK, Erkanli A, Peterson B, Oleson JR, et al. Oxygen and perfusion kinetics in response to fractionated radiation therapy in FaDu head and neck cancer xenografts are related to treatment outcome. Int J Radiat Oncol 2016;96:462–9.

18. Wang X, Wolfbeis OS. Optical methods for sensing and imaging oxygen: materials, spectroscopies and applications. Chem Soc Rev 2014;43:3666–761. [PubMed: 24638858]
19. Papkovsky DB, Dmitriev RI. Biological detection by optical oxygen sensing. Chem Soc Rev 2013;42:8700. [PubMed: 23775387]
20. Vinogradov SA, Lo LW, Jenkins WT, Evans SM, Koch C, Wilson DF. Noninvasive imaging of the distribution in oxygen in tissue in vivo using near-infrared phosphors. Biophys J 1996;70:1609–17. [PubMed: 8785320]
21. Esipova TV, Karagodov A, Miller J, Wilson DF, Busch TM, Vinogradov SA. Two new “protected” oxyphors for biological oximetry: properties and application in tumor imaging. Anal Chem 2011;83:8756–65. [PubMed: 21961699]
22. Zhang S, Hosaka M, Yoshihara T, Negishi K, Iida Y, Tobita S, et al. Phosphorescent light-emitting iridium complexes serve as a hypoxia-sensing probe for tumor imaging in living animals. Cancer Res 2010;70:4490–8. [PubMed: 20460508]
23. Zheng X, Mao H, Huo D, Wu W, Liu B, Jiang X. Successively activatable ultrasensitive probe for imaging tumour acidity and hypoxia. Nat Biomed Eng 2017;1:0057.
24. Zheng X, Wang X, Mao H, Wu W, Liu B, Jiang X. Hypoxia-specific ultrasensitive detection of tumours and cancer cells in vivo. Nat Commun 2015;6:5834. [PubMed: 25556360]
25. Napp J, Behnke T, Fischer L, Würth C, Wottawa M, Katschinski DM, et al. Targeted luminescent near-infrared polymer-nanoprobes for in vivo imaging of tumor hypoxia. Anal Chem 2011;83:9039–46. [PubMed: 22007722]
26. Lemon CM, Karnas E, Han X, Bruns OT, Kempa TJ, Fukumura D, et al. Micelle-encapsulated quantum dot-porphyrin assemblies as in vivo two-photon oxygen sensors. J Am Chem Soc 2015;137:9832–42. [PubMed: 26149349]
27. Wu C, Bull B, Christensen K, McNeill J. Ratiometric single-nanoparticle oxygen sensors for biological imaging. Angew Chemie Int Ed 2009;48:2741–5.
28. Shi H, Ma X, Zhao Q, Liu B, Qu Q, An Z, et al. Ultrasmall phosphorescent polymer dots for ratiometric oxygen sensing and photodynamic cancer therapy. Adv Funct Mater 2014;24:4823–30.
29. Pu K, Shuhendler AJ, Jokerst JV., Mei J, Gambhir SS, Bao Z, et al. Semiconducting polymer nanoparticles as photoacoustic molecular imaging probes in living mice. Nat Nanotechnol 2014;9:233–9. [PubMed: 24463363]
30. Borisov SM, Klimant I. Luminescent nanobeads for optical sensing and imaging of dissolved oxygen. Microchim Acta 2009;164:7–15.
31. Shuhendler AJ, Pu K, Cui L, Uetrecht JP, Rao J. Real-time imaging of oxidative and nitrosative stress in the liver of live animals for drug-toxicity testing. Nat Biotechnol 2014;32:373–80. [PubMed: 24658645]
32. Wilson DF. Oxygen dependent quenching of phosphorescence: a perspective. Adv Exp Med Biol 1992;317:195–201. [PubMed: 1288127]
33. Kizaka-Kondoh S, Konse-Nagasawa H. Significance of nitroimidazole compounds and hypoxia-inducible factor-1 for imaging tumor hypoxia. Cancer Sci 2009;100:1366–73. [PubMed: 19459851]
34. Knox HJ, Hedhli J, Kim TW, Khalili K, Dobrucki LW, Chan J. A bioreducible N-oxide-based probe for photoacoustic imaging of hypoxia. Nat Commun 2017;8:1794. [PubMed: 29176550]
35. Wilhelm S, Tavares AJ, Dai Q, Ohta S, Audet J, Dvorak HF, et al. Analysis of nanoparticle delivery to tumours. Nat Rev Mater 2016;1:16014.
36. Matsumoto S, Yasui H, Batra S, Kinoshita Y, Bernardo M, Munasinghe JP, et al. Simultaneous imaging of tumor oxygenation and microvascular permeability using Overhauser enhanced MRI. Proc Natl Acad Sci 2009;106:17898–903. [PubMed: 19815528]
37. Detmar M, Brown LF, Berse B, Jackman RW, Elicker BM, Dvorak HF, et al. Hypoxia regulates the expression of vascular permeability factor/vascular endothelial growth factor (VPF/VEGF) and its receptors in human skin. J Invest Dermatol 1997;108:263–8. [PubMed: 9036922]
38. Kallman RF, Dorie MJ. Tumor oxygenation and reoxygenation during radiation therapy: their importance in predicting tumor response. Int J Radiat Oncol Biol Phys 1986;12:681–5. [PubMed: 3700172]

39. Rubin P, Casarett G. Microcirculation of tumors. I. Anatomy, function, and necrosis. Clin Radiol 1966;17:220–9. [PubMed: 5942772]
40. Liu SS. Enhancement of the radiosensitivity of cervical cancer cells by overexpressing p73. Mol Cancer Ther 2006;5:1209–15. [PubMed: 16731753]
41. Kim KH, Yoo HY, Joo KM, Jung Y, Jin J, Kim Y, et al. Time-course analysis of DNA damage response-related genes after in vitro radiation in H460 and H1229 lung cancer cell lines. Exp Mol Med 2011;43:419. [PubMed: 21633183]
42. Benej M, Hong X, Vibhute S, Scott S, Wu J, Graves E, et al. Papaverine and its derivatives radiosensitize solid tumors by inhibiting mitochondrial metabolism. Proc Natl Acad Sci 2018;115:10756–61. [PubMed: 30201710]
43. Zhang HF, Maslov K, Stoica G, Wang L V. Functional photoacoustic microscopy for high-resolution and noninvasive in vivo imaging. Nat Biotechnol 2006;24:848–51. [PubMed: 16823374]
44. Pauling L, Coryell CD. The magnetic properties and structure of hemoglobin, oxyhemoglobin and carbonmonoxyhemoglobin. Proc Natl Acad Sci 1936;22:210–6. [PubMed: 16577697]
45. Brizel DM, Sibley GS, Prosnitz LR, Scher RL, Dewhirst MW. Tumor hypoxia adversely affects the prognosis of carcinoma of the head and neck. Int J Radiat Oncol 1997;38:285–9.
46. Dewhirst MW, Secomb TW. Transport of drugs from blood vessels to tumour tissue. Nat Rev Cancer 2017;17:738–50. [PubMed: 29123246]
47. Fajardo LFL-G. Ionizing radiation and the endothelium Late Eff Cancer Treat Norm Tissues. Berlin, Heidelberg: Springer Berlin Heidelberg; page 19–22.
48. Kallman RF. The phenomenon of reoxygenation and its implications for fractionated radiotherapy. Radiology 1972;105:135–42. [PubMed: 4506641]

Significance

This study presents a novel nano-agent for the visualization and quantification of tumor hypoxia.

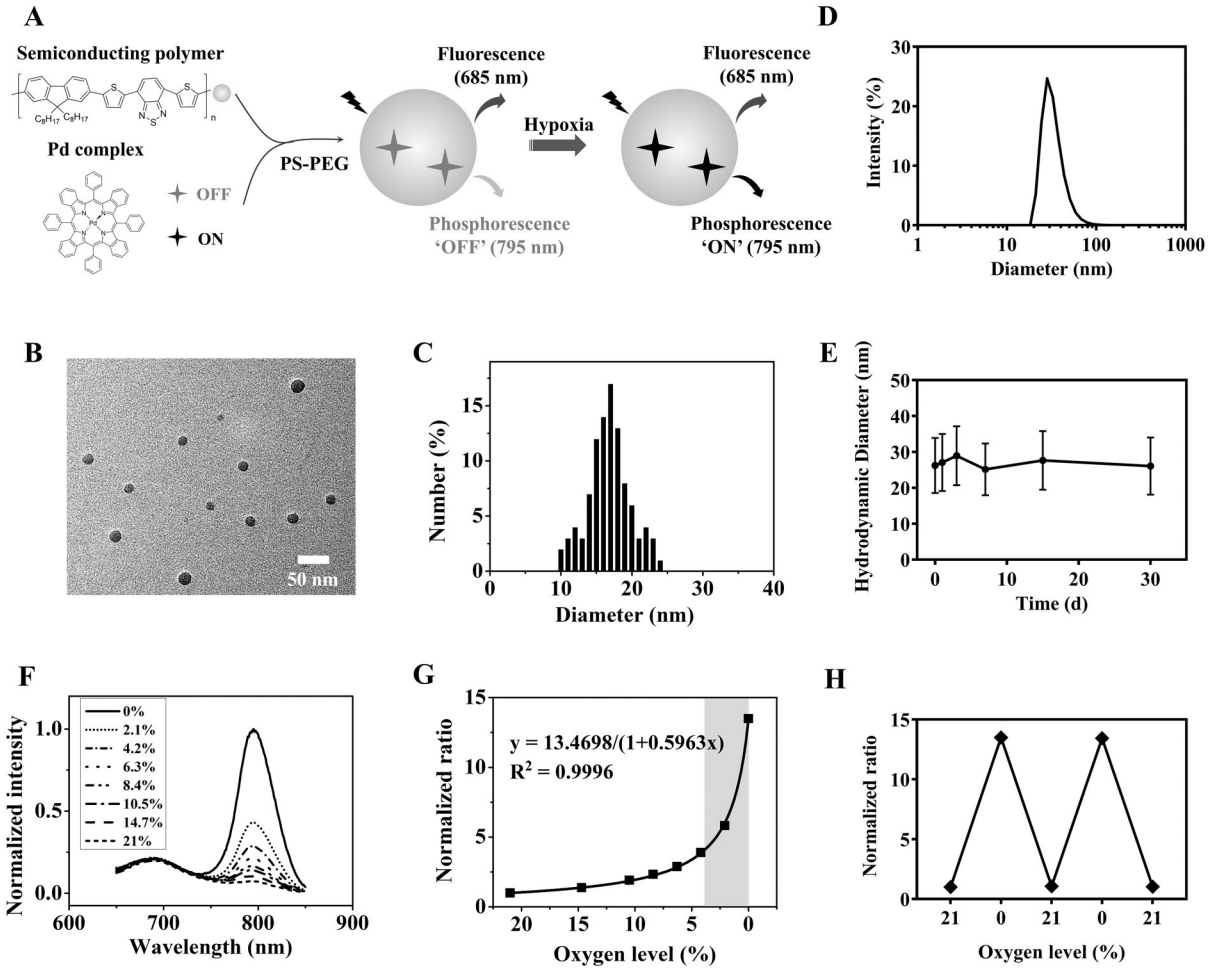

Figure 1.

Synthesis and photophysical properties of the nanoprobe. **A,** Design of the RHyLI nanoprobe and its hypoxia sensing mechanism. **B,** A representative TEM image of the nanoprobe. **C,** Size distribution of the nanoprobe under TEM. **D,** Hydrodynamic diameter of the nanoprobe in distilled water by DLS. **E,** Stability test of the nanoprobe in PBS (1×, pH 7.4). Results are presented as mean ± SD (N = 3). **F,** Emission spectra of the RHyLI nanoprobe in distilled water (5 μg/mL) at various oxygen levels (0-21%). Excitation: 630 nm. **G,** The ratio between the emission intensities at 795 and 685 nm at various oxygen levels. The region of oxygen level related to tumor resistance to RT is highlighted. **H,** Reversible response of the nanoprobe to the change of oxygen level.

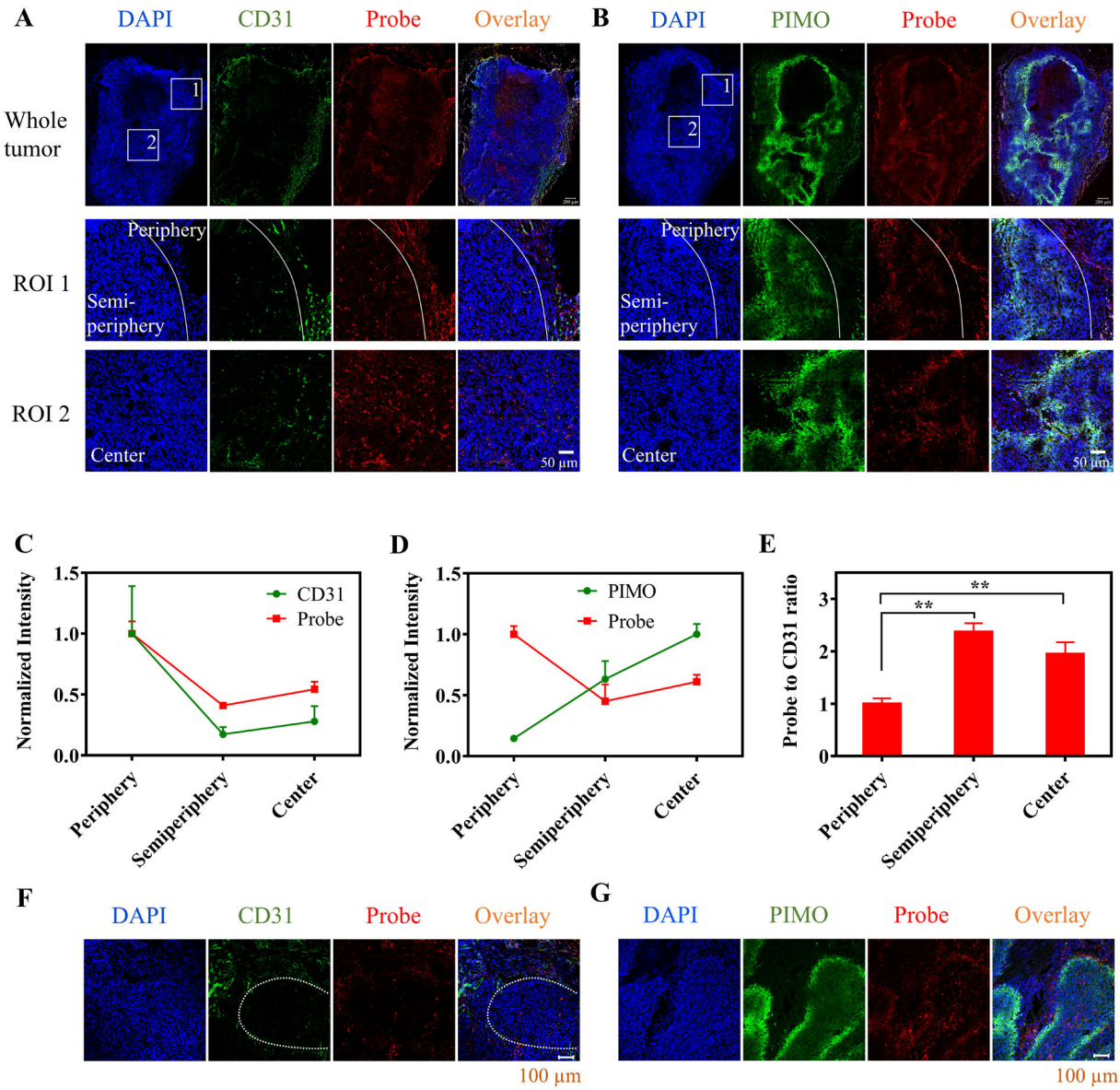

Figure 2.

Intratumor distribution of the nanoprobe after i.v. injection. **A,B,** Nude mice bearing HeLa tumor were i.v. injected with the nanoprobe (2 mg/kg) and the tumor tissues were collected at 24 h p.i. The frozen sections of the tumor tissues were stained with (**A**) CD31 antibody and (**B**) pimonidazole (PIMO) antibody (green). The nanoprobe was observed by collecting its 685 nm emission (red) and nuclei of cells were stained with DAPI (blue). Two regions of interest (ROIs) in the whole tumor sections were selected and enlarged in bottom two rows (white boxes). ROI 1 contained two regions as divided by the white line: the tumor periphery on the right side and semi-periphery (0–400 μm to the periphery) on the left side; ROI 2 was in the center of the tumor. Scale bars: 200 μm for whole tumor and 50 μm for the ROIs. **C,D,E,** The probe distribution in three different regions of the tumor tissues (periphery, semi-periphery, and center) is compared to levels of (**C**) vascular density (CD31 staining intensity per area) or (**D**) hypoxia (PIMO staining intensity per area). The signal intensities

per area of the probe, CD31 and PIMO in various regions were normalized by the average probe signal intensity per area in the periphery, average CD31 staining intensity per area in the periphery, and average PIMO staining intensity per area in the center, respectively. **E**, The ratios of probe concentration to vascular density in the three different regions were compared. Results are presented as Mean ± SD (N = 3). ** $p < 0.01$, in comparison among the probe-to-CD31-ratio values of various tumor regions by one-way ANOVA with Geisser-Greenhouse correction. **F,G,** Penetration of the nanoprobes from the blood vessels to the hypoxic regions of the tumor tissue. The hypoxic regions were determined by (**F**) low vascular density or (**G**) PIMO staining. The white dashed line in **F** indicates a hypoxic region.

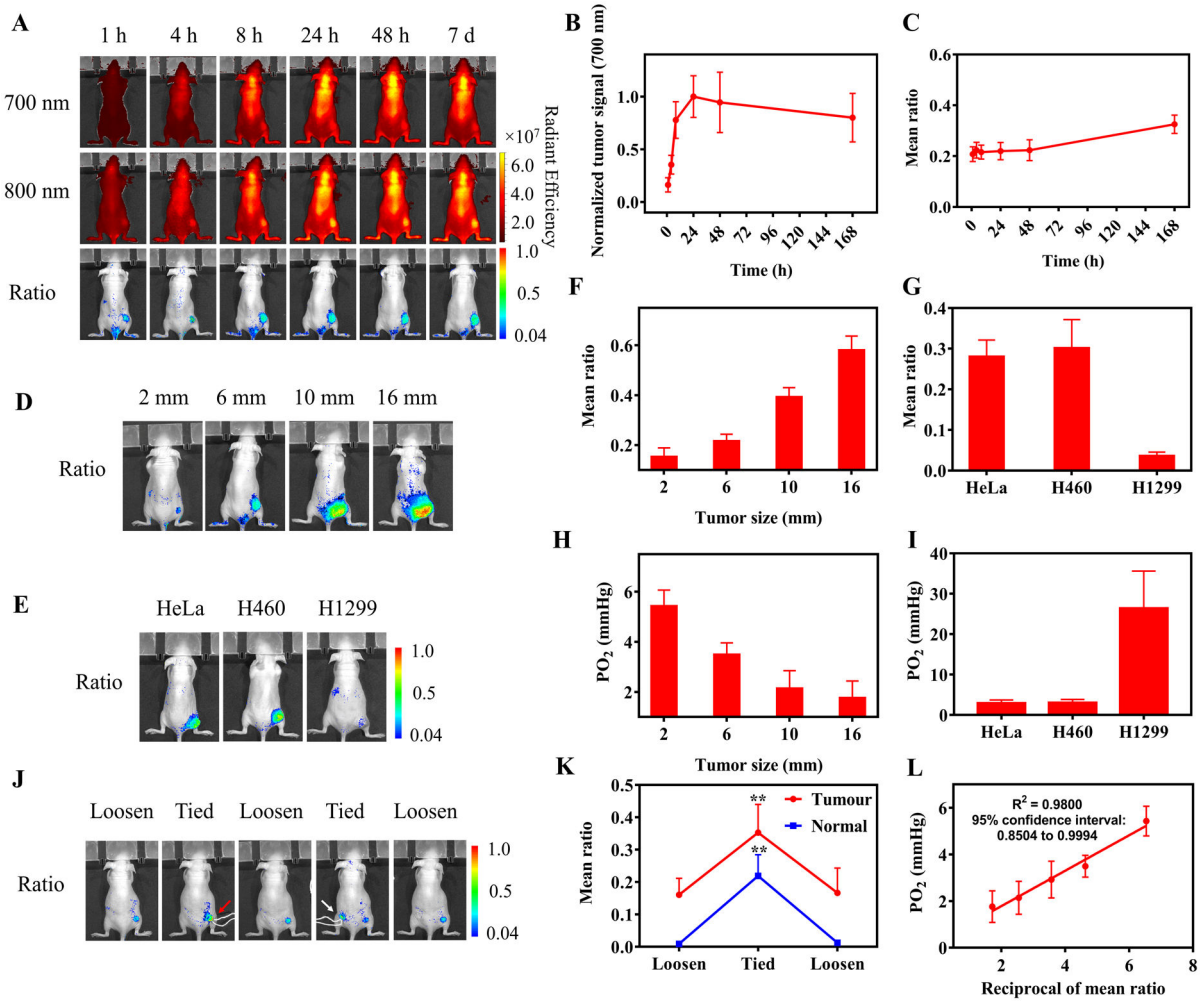

Figure 3.

Ratiometric imaging of tumor hypoxia after i.v. injection of the nanoprobe. **A,** Nude mice bearing HeLa tumor (6 mm) on the right rear thigh were i.v. injected with RHyLI (2 mg/kg) and imaged by ratiometric imaging over time. **B,** The tumor signal intensities in the 700 nm channel in **A** show the accumulation and retention of the nanoprobe in the tumor tissues over 7 days. **C,** Plot of the values of the mean ratio (the mean signal intensity of all the pixels in the tumor region) for the tumor in the ratiometric images in (**A)** versus time. **D-I,** Ratiometric imaging of hypoxia in tumors with indicated size or type. Nude mice bearing (**D**) HeLa tumors with a size of 2, 6, 10, or 16 mm (N = 3 for each group), or (**E**) HeLa, H460, or H1299 tumor with a size of 8 mm (N = 3 for each group) were i.v. injected with the nanoprobe (2 mg/kg) and imaged at 24 h p.i. **F,G,** The values of mean ratio of tumors in the ratiometric images. **H,I,** Partial oxygen pressure (PO_2) in tumors in (**D,E**) measured by the needle-type oxygen microelectrode. **J,K,** Reversible response of the nanoprobe to hypoxia. Nude mice bearing HeLa tumor (2 mm) were i.v. injected with the nanoprobe (2 mg/kg). At 24 h p.i., the tumor tissue on the right thigh (red arrow) or the normal tissue on the left thigh (white arrow) was tied with a string to induce the temporal increase of hypoxia and then untied for the recovery of blood circulation. (**J**) Mice were monitored by ratiometric imaging

and (**K**) tumor hypoxia in the ratiometric images was quantified by the values of mean ratio. Results are presented as Mean ± SD (N = 3). ** $p < 0.01$, when comparing the mean ratio values of the tied state with those of loosen states by one-way ANOVA with Geisser-Greenhouse correction. **L,** Correlation of the reciprocal of the mean ratio with the corresponding oxygen partial pressure measured by the oxygen microelectrode. The values of mean ratio and PO_2 used for correlation are the measurement results of HeLa tumors at various tumor sizes by ratiometric imaging (**F,G**) and oxygen microelectrode (**H,I**).

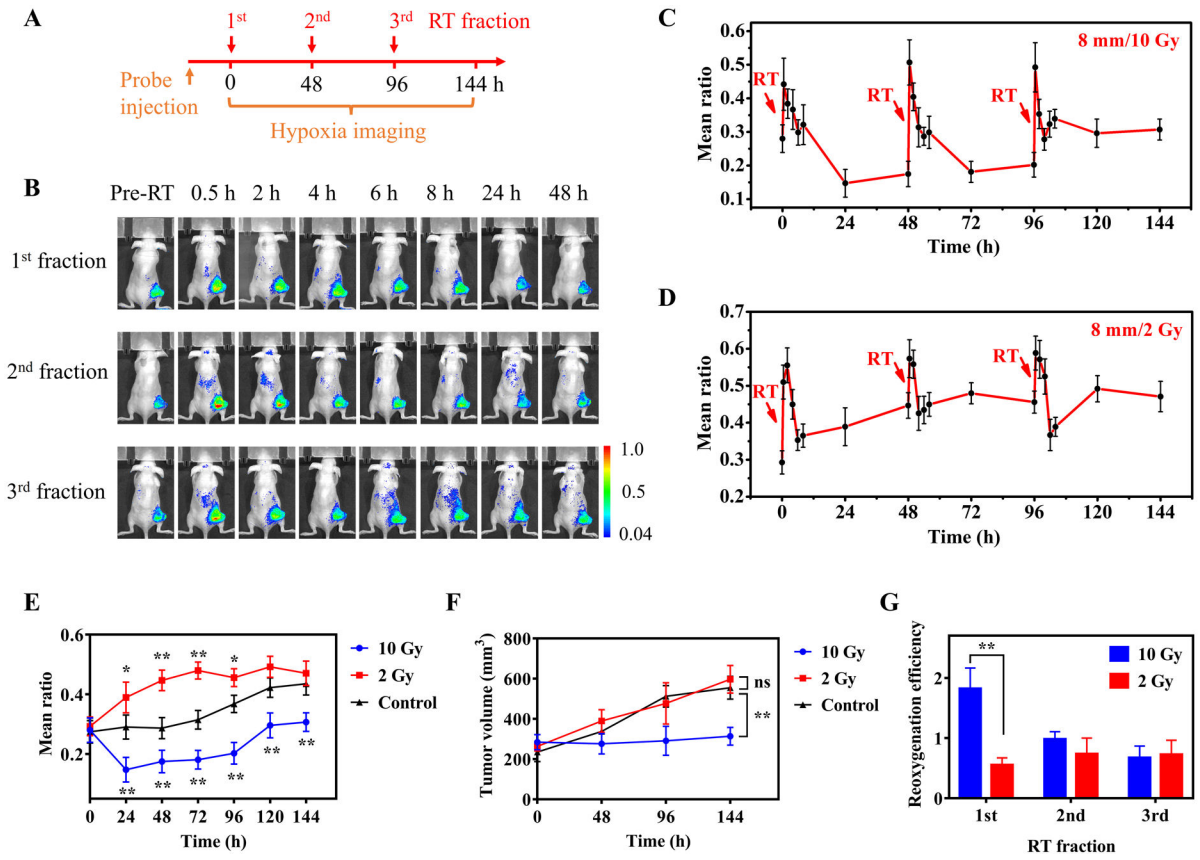

Figure 4.

Real-time monitoring tumor hypoxia dynamics in fractionated RT. **A,** Timeline of the experiment. Tumor-bearing mice were treated with three RT fractions with a 48 h interval. The nanoprobe was i.v. injected to the mice (2 mg/kg) at 24 h before the first RT fraction. Tumor hypoxia was imaged before RT and at 0.5 to 48 h after each RT fraction. **B,** Ratiometric images of a mouse bearing a HeLa tumor (8 mm) at indicated time points during three RT fractions (10 Gy per fraction). **C,D,** Evolution of the mean ratio over time when HeLa tumors (8 mm) were treated with three RT fractions (**C**: 10 Gy; **D**: 2 Gy per fraction; N = 3 per group). **E,** Long-term evolution of tumor hypoxia measured with a 24 h interval in HeLa tumors (8 mm) received indicated RT doses (10, 2, and 0 Gy as control). Results are presented as Mean ± SD (N = 3). * $p < 0.05$, ** $p < 0.01$, when comparing the mean ratio values of the RT-treated groups with those of the control group at various time points by one-way ANOVA with Geisser-Greenhouse correction. **F,** Tumor growth curves of HeLa tumors (8 mm) treated with different RT doses (10, 2 and 0 Gy as control). ** $p < 0.01$, 'ns' (not significant) $p > 0.05$, when comparing the tumor volumes of the RT-treated groups with those of the control group at 144 h time point by one-way ANOVA with Geisser-Greenhouse correction. **G,** Reoxygenation efficiency, defined by the ratio of hypoxia decrease in 0.5–24 h (the difference between the mean ratio at 0.5 h and 24 h) to hypoxia increase in 0–0.5 h after each RT fraction (the difference between the mean ratio between 0.5 h and pre-RT) of HeLa tumors for each RT fraction at different RT doses. Results are presented as Mean ± SD

(N = 3). ** $p < 0.01$, in comparison between the reoxygenation efficiencies under different RT doses in the 1st RT fraction by two-tailed t-test with Welch's correction.

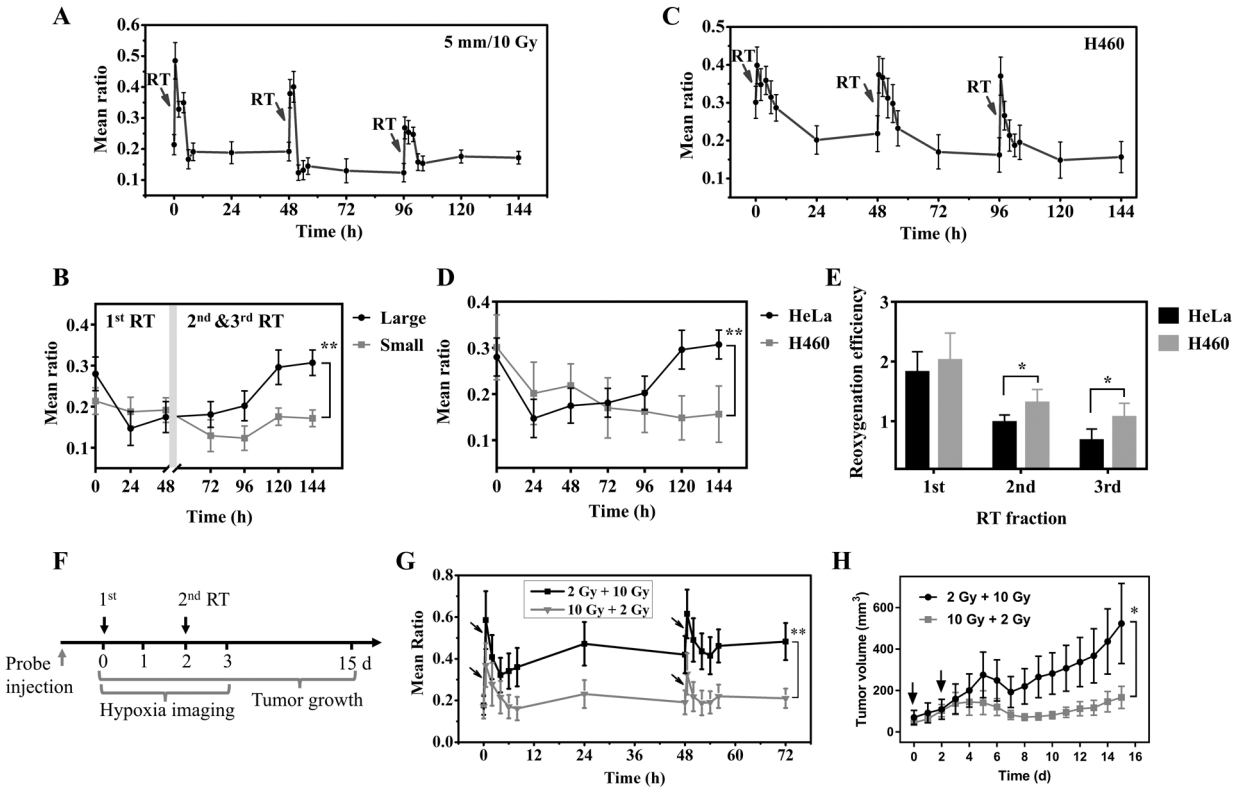

Figure 5 |.

Tumor hypoxia dynamics in RT at different tumor size/type and the effect of the first fraction dose on tumor hypoxia dynamics and treatment outcome. **A,C,** Evolution of tumor hypoxia over time when nude mice bearing (**A**) HeLa tumor (5 mm) or (**C**) H460 tumor (8 mm) were treated with three RT fractions (10 Gy per fraction). **B,D,** Comparison of the long-term evolution of hypoxia of (**B**) HeLa tumors with indicated size (large: 8 mm; small: 5 mm) or (**D**) different tumor types (HeLa or H460) at the same tumor size (8 mm). Results are presented as Mean ± SD (N = 3). ** $p < 0.01$, in comparison between the mean ratio values at different (**B**) tumor sizes or (**D**) tumor types at 144 h time point by two-tailed t-test with Welch's correction. **E,** The reoxygenation efficiency of HeLa and H460 tumors in each RT fraction. Results are presented as Mean ± SD (N = 3). * $p < 0.05$, in comparison between the reoxygenation efficiency of HeLa and H460 tumors in the 2nd and 3rd RT fraction by two-tailed t-test with Welch's correction. **F,G,H,** The effect of first fraction dose on tumor hypoxia dynamics and treatment outcome. (**F**) Timeline of the experiment. Nude mice bearing H460 tumors were treated with two RT fractions at day 0 and day 2 (group 1: 2 Gy + 10 Gy, group 2: 10 Gy + 2 Gy, n = 10 per group). The nanoprobe was i.v. injected to the mice (2 mg/kg) at 24 h before the first RT fraction. (**G**) The evolution of tumor hypoxia was monitored from day 0 to day 3 and (**H**) the tumor growth was recorded from day 0 to day 15. The black arrows indicate RT treatment. * $p < 0.05$, ** $p < 0.01$, in comparison between the (**G**) mean ratio or (**H**) tumor volume of the two groups by two-tailed t-test with Welch's correction.